coatings

MDPI

Article

# Investigating Hydrogen Separation in a Novel Rotating Carbon Nanotube–Carbon Nanocone Setup Using Molecular Dynamics Simulations

**Sorin Muraru [1,*,†], Sebastian Muraru [1,2,*] and Mariana Ionita [1,2,†]**

[1] Advanced Polymer Materials Group, University Politehnica of Bucharest, Gh Polizu 1-7, 011061 Bucharest, Romania; mariana.ionita@polimi.it

[2] Faculty of Medical Engineering, University Politehnica of Bucharest, Gh Polizu 1-7, 011061 Bucharest, Romania

* Correspondence: sor.muraru@gmail.com (S.M.); sebmuraru@gmail.com (S.M.)

† These authors contributed equally to this work.

Received: 20 November 2020; Accepted: 7 December 2020; Published: 10 December 2020


**Abstract:** Hydrogen fuel cells rely on the purity of the hydrogen gas for maintaining a high performance. This study investigates a novel nanostructure design for its effectiveness in separating $H_2$ molecules from a mixture of gases containing $H_2$, $CH_4$, $CO_2$, $N_2$, CO and $H_2O$ molecules using Molecular Dynamics simulations. Based on an open-ended (28, 0) rotating carbon nanotube with one carbon nanocone at each of its two extremes, this device is predicted through Molecular Dynamics simulations to be able to separate hydrogen from a gas mixture contained within. The nanocones were placed with their tips inside the nanotube and the size of the open channel created between the two was controlled to find a configuration that allows hydrogen to pass while restricting the other gases. Although in need of optimization, we find it capable of high selectivity and highlight captivating gas behavior insights to help advance rational gas separation device development.

**Keywords:** hydrogen separation; Molecular Dynamics; carbon nanotube; carbon nanocone

## 1. Introduction

Gas separation is an increasingly engaged topic amidst researchers for its wide range of applications. Among these, hydrogen fuel cells are actively researched for their potential to conveniently and efficiently convert chemical energy into electric energy given a continuous flow of elemental feed [1]. However, the latter can strongly diminish their performance due to the presence of other gas molecules, such as $CH_4$, $CO_2$, $N_2$, CO or $H_2O$, which are commonly found in the steam reforming process. These additional gases can affect the metal catalyst that promotes the electrochemical reactions [2]. It is imperatively necessary to maintain hydrogen purity and separate the other polluting gas molecules.

Carbon, with its many allotropes and unmatched versatility, has constantly been a significant point of interest for the Materials Science researchers. Discovery of new allotropes, showing unique properties, has made it useful in a large spectrum of applications. In particular, carbon nanotubes and graphene have received increased attention in gas separation studies. Super carbonaceous structures are composite carbon nanostructures formed from at least two carbon allotropes. Rotational motion of double walled carbon nanotubes was recently observed when these were exposed to an electric field [3], opening the door to imagining super carbonaceous nanomotors as filtration devices.

The field of gas separation is dominated by computational studies, which are used both for prediction of performance and understanding of the mechanisms involved. Computational studies have predicted through theoretical simulations that hydrogen can pass the energy barrier imposed by a graphene pore of a diameter as small as 1.95 Å if given enough time [4]. Analogously, all the molecules

from the considered gas mixture that may contaminate pure hydrogen, such as $CH_4$, $CO_2$, $N_2$, CO and $H_2O$, have been predicted to go through graphene-based membranes with pores of different sizes and shapes or specific interlayer spacing [4–15]. The larger lot of these predictions has been reached using the computational method of Molecular Dynamics. This uses classical physics laws to study the trajectories of gas molecules through separation membranes [16]. This method can be used for gaining new insights on the behavior of systems at a nano-perspective that are inconvenient to study practically. Ultimately, the level of detail provided by Molecular Dynamics simulations cannot be matched experimentally. Performance of carbon-based structures has been previously investigated solely through Molecular Dynamics simulations both for filtration applications such as gas separation [17–24] and water desalination [25,26].

In this study, we make use of Molecular Dynamics simulations to explore hydrogen separation out of a mixture containing $H_2$, $H_2O$, $N_2$, CO, $CO_2$ and $CH_4$ molecules in a novel super carbonaceous nanomotor design. The analyzed nanostructure is made out of the following elements: a rotating carbon nanotube acting as a container for the gas molecules surrounded at the middle by a shorter steady carbon nanotube of a larger diameter, and two carbon nanocones at the open ends of the longer carbon nanotube with their tips inside it, each adsorbed to a graphene sheet at its base. The rationale of this system is that the rotative motion would send the gas molecules out, towards the open ends of the carbon nanotube and, given the right amount of energy, hydrogen molecules will exit through the gap formed between the carbon nanotube and the carbon nanocones. We provide a total of ten simulations as study cases, five at 300 K and five at 450 K, slightly varying the positioning of the carbon nanocones on the *Z*-axis and thus changing the area of the gap. We found that high selectivity for $H_2$ can be reached and discuss captivating insights meant to help in developing future solutions stemming from our original design. From an experimental perspective, the rotating motion of the inner carbon nanotube could be generated by the presence of an electric field, while during our simulations it is due to an imposed angular velocity of $\omega = 180°$ $ps^{-1}$.

## 2. Materials and Methods

### *2.1. Design Setup*

The design of the proposed setup is shown in Figure 1. A central zigzag carbon nanotube of chiral indices (28, 0) and 12.6 nm in length was placed between two identical carbon nanocones of disclination 120° with their tips pointing inside the aforementioned structure. These were distanced at least 11.5 nm and at most 11.8 nm apart as measured from tip to tip and were generated in Nanotube Modeler [27] with a very large height. They were then cut to the right size by counting the number of hexagonal rings below its tip as shown in Figure 2, as further explained in *Nanocone Generation*. A second carbon nanotube 5 nm in length was placed as a double wall at the center of the zigzag carbon nanotube. The setup was locked between two graphene sheets of 10 nm × 10 nm placed 15 nm apart. An angular velocity $\omega = 180°$ $ps^{-1}$ was imposed on the central carbon nanotube to allow it to rotate. The outer 5 nm carbon nanotube, the two carbon nanocones and the graphene sheets were all positionally restrained. A total of 150 gas molecules were placed randomly in the middle of the central carbon nanotube, meaning 100 $H_2$, 20 $CH_4$, 10 $CO_2$, 10 CO, 10 $N_2$ and 10 $H_2O$ molecules, a mixture used in previous studies on hydrogen separation [23,24]. Five main scenarios were simulated at 300K with varying sizes of the gaps between the carbon nanocones and the carbon nanotube for 10 ns. In addition, a second set of another five cases were simulated at 450 K for 5 ns. For details please see the Results section (Section 3).

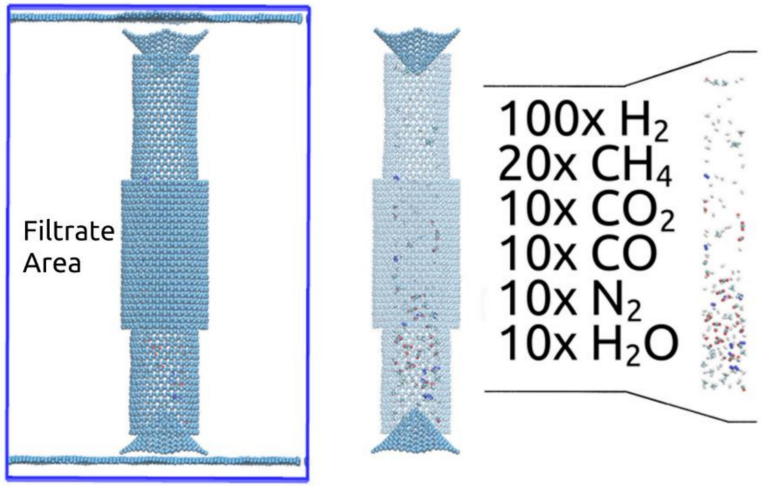


**Figure 1.** The overall setup of the investigated design, relying on a rotating central carbon nanotube (28, 0) 12.6 nm in length, partially double-walled by a 5 nm long (19, 19) secondary carbon nanotube, with two carbon nanocones placed with their tip inside the inner nanotube and the filtrate area shielded by two 10 nm × 10 nm graphene sheets. The mixture of gases placed inside the setup is shown on the right.

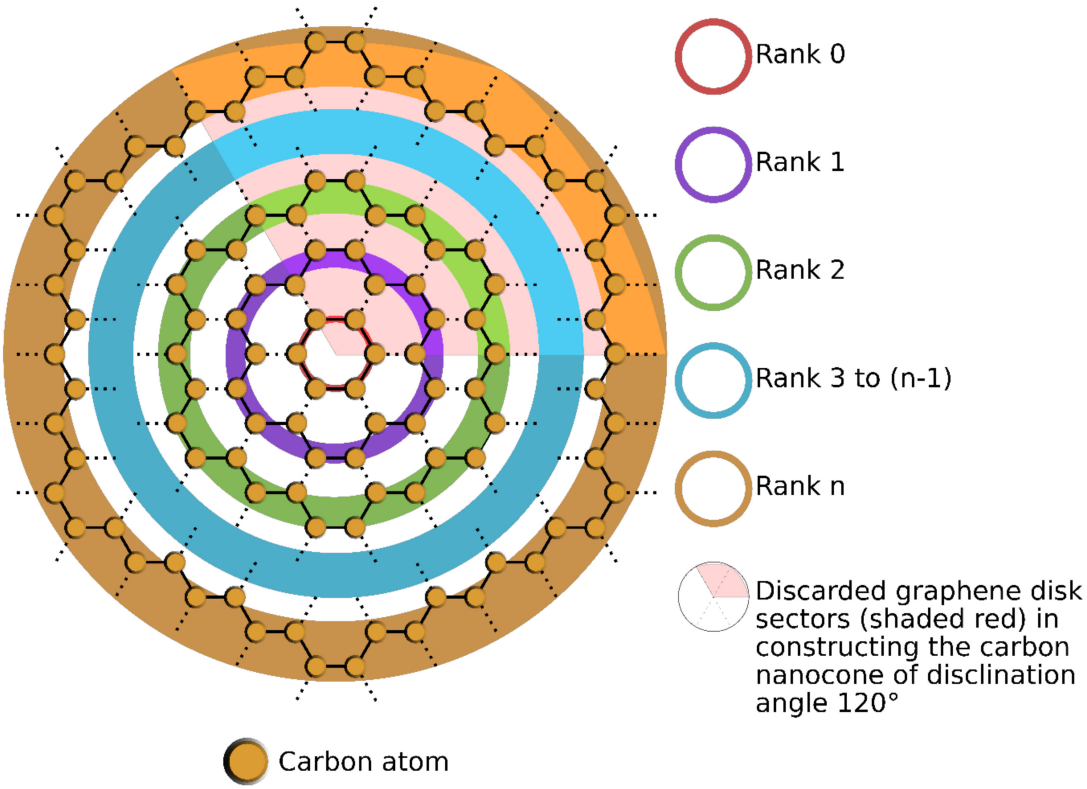


**Figure 2.** Construction of the carbon nanocone based on the necessary rank number as viewed on a graphene nanodisk.

### 2.2. Nanocone Generation

Generation of the correct size carbon nanocones is shown in Figure 2. Usually, carbon nanocones are rolled up circular graphene nanodisks, from which up to 5 sectors are removed, each corresponding to 60°. The total angle of the sliced out sectors is called the disclination angle. The preceeding figure shows chains or loops of sideways connected carbon atoms, which for convenience are numbered from rank 0 to an arbitrary rank n. Starting from the center of the graphene nanodisk, once a rank has

been found to be able to generate a larger diameter than the one of the carbon nanotube, all carbon nanocones of that specific rank or higher become compatible for our nanostructure. Otherwise, if the base diameters of the carbon nanocones were smaller than the one of the carbon nanotube, the structure would have no stable support and the central piece may deviate from its position either upwards or downwards. All the carbon nanocones used in this nanostructure have a loop rank of 8 and a disclination angle of 120° as shown in Figure 3.

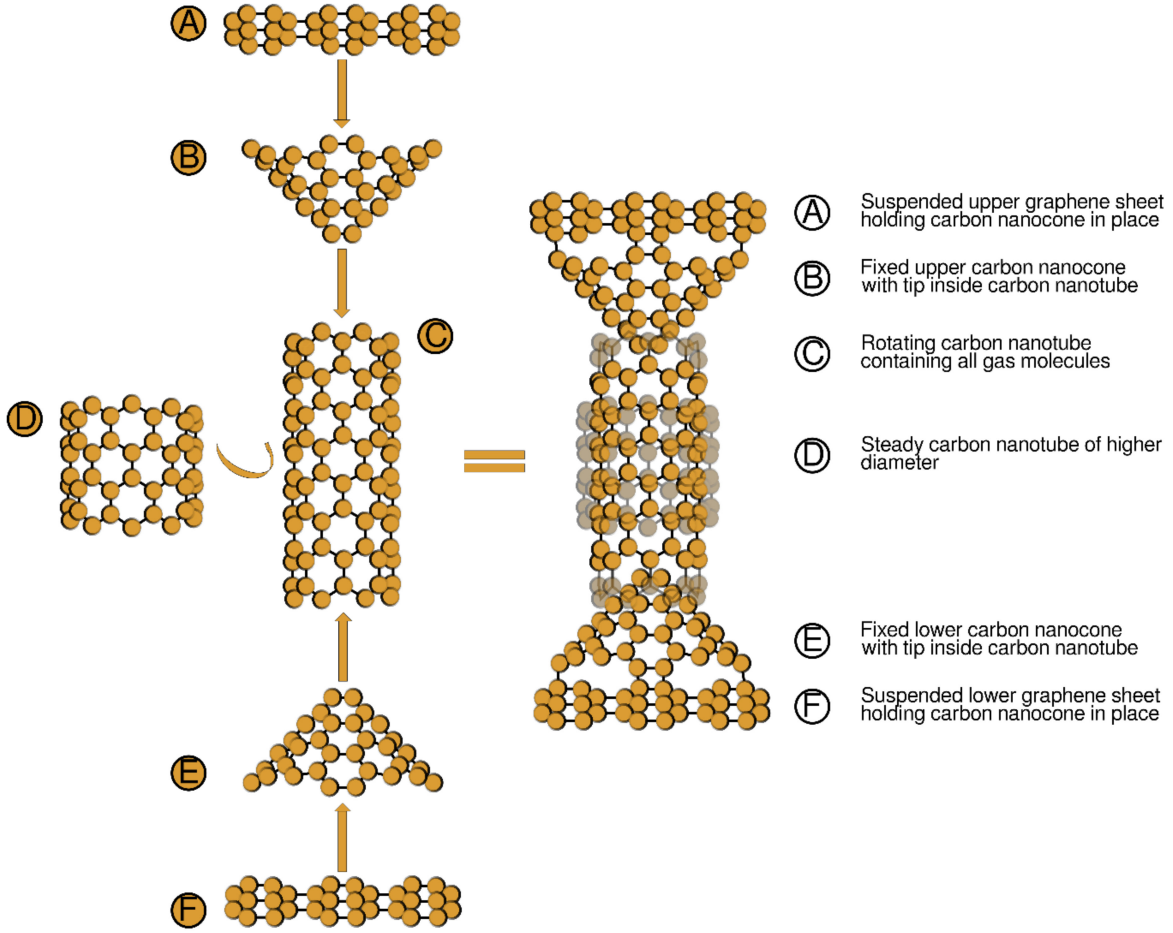


**Figure 3.** Supercarbonaceous structure used for gas separation with its individual components.

### *2.3. Simulation Details*

The simulations were run using the GROMACS 2018 engine [28] and the OPLS-AA forcefield [29]. The imposed angular velocity of $\omega = 180°$ ps$^{-1}$ on the central carbon nanotube was applied using the Enforced Rotation module and flex-2t potential. The rotational force constant was 500 kJ mol$^{-1}$ nm$^{-2}$. Positional restraints were applied on the outer 5 nm carbon nanotube, two carbon nanocones and the two graphene sheets. Energy minimization was performed using the steepest descent algorithm and was followed by a 1 ps NVT equilibration step. All simulations were run at a step size of 0.5 fs in an NVT ensemble, summing up to a total of 10 ns for the simulations ran at 300 K and 5 ns for the simulations ran at 450 K. Coordinates for visualizations were saved every 5 fs. Simulation box size was 10.2 nm × 10.2 nm × 16 nm and contained almost 14,200 atoms. Periodic boundary conditions were active in all directions. Graphene sheets of size 10 nm × 10 nm acted as boundaries in the Z-direction for all gases. The water model was SPC/E [30]. The Verlet cut-off scheme was used, together with the V-Rescale [31] thermostat.

Most parameters for the gas molecules were taken from previous studies using the OPLS-AA forcefield [22]. $H_2$ and $N_2$ molecules were modeled as three-site models, with one virtual mass-less

atom in the center of the molecules, while $CO_2$ molecules were built as a five-site model, thus using two virtual atoms, as shown in Lemkul's tutorial [32]. $CH_4$ and CO molecules were built without the aid of virtual atoms and thus contained five, respectively two atoms.

All carbon atoms defining the setup were modeled as uncharged LJ spheres of 0.34 nm cross section and 0.36 kJ $mol^{-1}$ potential wall depth. The C-C bond length was set at 1.42 Å, the bending angle between three carbon atoms was considered 120° and the C-C-C-C planar angles were maintained with the help of harmonic potentials. The springs constants of the latter were set at 322.55 kcal $mol^{-1}$ $Å^{-2}$, 53.35 kcal $mol^{-1}$ $rad^{-2}$ and 3.15 kcal $mol^{-1}$ [33]. The obtained data were analyzed in Python 3.7, using libraries such as NumPy, bokeh [34] and MDAnalysis [35].

## 3. Results

The novel promising design, shown in Figure 1, is defined by the two carbon nanocones situated at the ends of a (28, 0) rotating carbon nanotube. It is significantly different from setups used in comparable studies involving rotating carbon nanotubes for filtration purposes making use of nanopores [36]. To our best knowledge there are no similar setups investigating gas separation or gas behavior, thus we believe we open the door for new and more creative Molecular Dynamics investigations. The investigated gas mixture includes 100 $H_2$ molecules, 20 $CH_4$ molecules, 10 $CO_2$ molecules, 10 CO molecules, 10 $N_2$ molecules and 10 $H_2O$ molecules.

### *3.1. Nanoslit Areas*

Throughout all our simulations, one end of the nanotube was consistently found too close to one of the carbon nanocones to allow for any of the gas molecules to exit, leaving only one side involved in the filtration process. In order to provide an estimate for the space between the end of the nanotube at which the molecules could exit and the nearby carbon nanocone (which we call the nanoslit), we made use of a Monte-Carlo hit-and-miss procedure [18,20,22] considering the effective carbon atom radius $R_{eff} = R_{m,c}/\sqrt{2}$ and $R_{m,c}$ equal to 0.17 nm. We calculated the areas by taking a slice of the atoms present at the exit-allowing end of the nanotube. The approximate results are shown numerically nearby each simulation and the area of interest is displayed in blue (images not in scale).

The ten study cases are presented in Figure 4A–E and Figure 5A–E. Five of the simulations were ran at 300 K for 10 ns and five others at 450 K for 5 ns. Due to the small 1 ps NVT equillibration step of the whole system and the enforcing of an angular velocity $\omega = 180°$ $ps^{-1}$ on the carbon nanotube during the simulations, the geometrical center of the tube moved slightly on the *Z*-axis compared to the its position after the energy minimization step (between 1–2 Å). This lead to the seemingly random nanoslit areas and their respective numerical estimates shown in Figures 4 and 5. Given our original design, we observed several key insights that should allow future studies to build upon and investigate with novel membranes and nanomotors with applications in hydrogen separation.

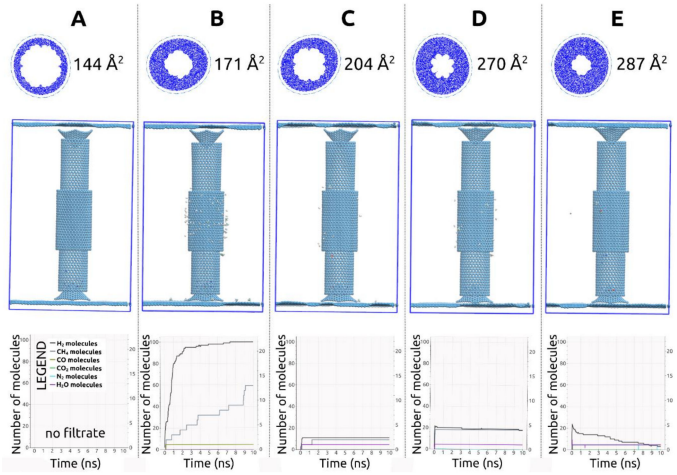


**Figure 4.** The results of the five study cases run at 300 K, which include a graphical representation and a numerical estimation of the nanoslit area, a final snapshot of the simulation and the graph showing the evolution of the number of gas molecules in the filtrate area with time. Graph legend is shown in the first graph (no filtrate).

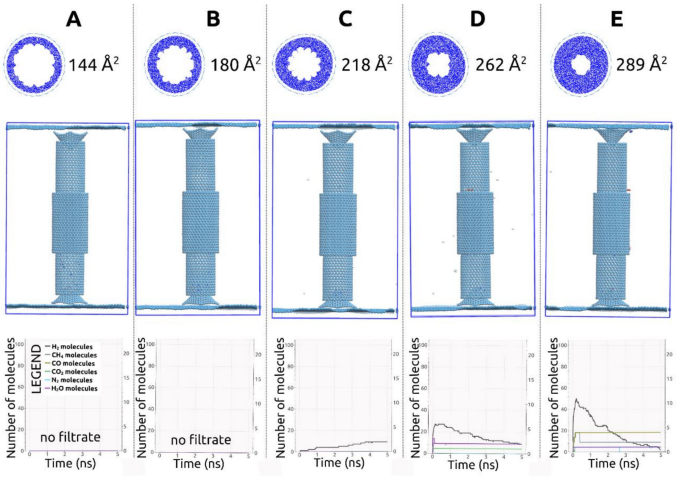


**Figure 5.** The results of the five study cases run at 450 K, which include a graphical representation and a numerical estimation of the nanoslit area, a final snapshot of the simulation and the graph showing the evolution of the number of gas molecules in the filtrate area with time. Graph legend is shown in the first graph (no filtrate).

### *3.2. The Role of the Applied Position Restraints*

Given the manner in which the system was built, the nanocones were adsorbed to the nearest graphene sheet due to π-π stacking interactions. However, given their position relative to the rotating carbon nanotube, they were also influenced by its motion through van der Waals interactions. In this study, we have used the position restraints to be able to test our nanodevice and keep the centers of the nanocones and the center of the nanotube colinear. Running simulations without the applied position restraints leads to the scenarios shown in Figure 6.

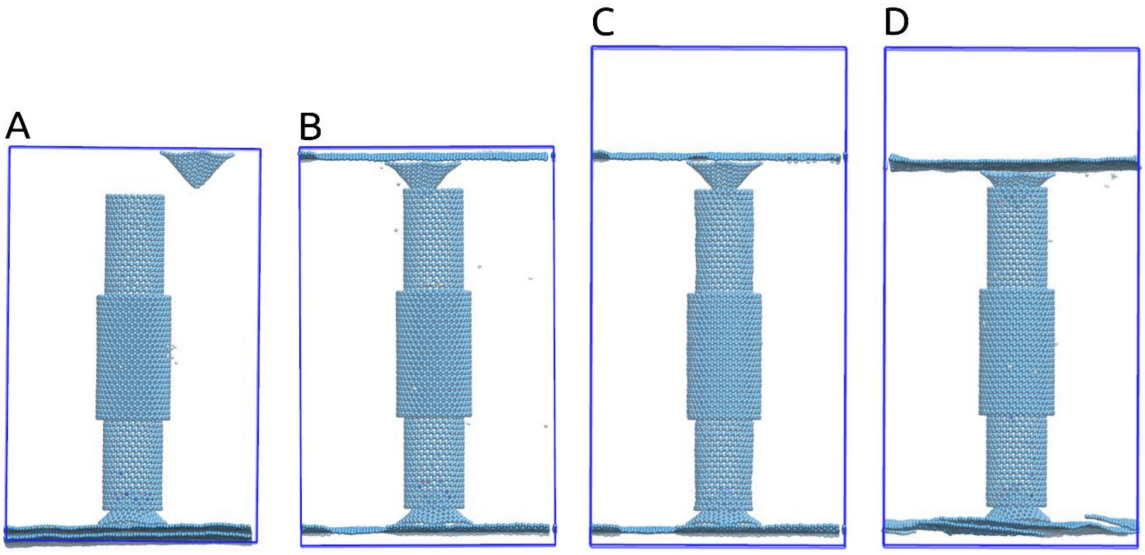


**Figure 6.** (**A**) Simulation without position restraints; (**B**) simulation with position restraints applied only to the graphene sheets; (**C**) simulation without position restraints and enlarged simulation box on the *Z*-axis; (**D**) same simulation as C showing that one of the carbon nanocones has changed its position relative to the carbon nanotube.

Thus, running without any position restraints, given the active periodic boundary conditions in all directions and the simulation box at the edges of which the graphene sheets were placed, one graphene sheet was able to move towards the other sheet until the two were adsorbed to each other. The nanocone adsorbed to the graphene sheet was dragged along, leaving one end of the nanotube entirely free, as shown in Figure 6A.

Applying position restraints to the graphene sheets alone, given the rotational movement of the nanotube, one of the nanocones was able to slightly change its position relative to the nanotube on the XY direction despite being adsorbed to the graphene sheet, as shown in Figure 6B. This ruined the control one would have over both the nanoslit area and the collinearity between the center of the carbon nanotube and the center of the carbon nanocones.

Running without any position restraints, yet with a larger box on the Z-axis, both nanocones remained with their tip inside the nanotube, however as the graphene sheets undulated slightly, the nanocones moved as well, which again lead to a change in the nanoslit area and disappearance of collinearity, as shown in Figure 6C,D, which belong to the same simulation.

### *3.3. The Role of the Imposed Angular Velocity*

The imposed angular velocity helped the rotating carbon nanotube maintain its shape throughout the simulation and thus allowed for some degree of control for keeping the nanoslit circular, as opposed to distorted. On top of that, given the rotational motion, adsorption of the gas molecules to the walls of the inner rotating carbon nanotube is slightly prevented and thus, through collisions, gas molecules are more likely to move while inside.

### *3.4. 300 K Study Cases*

Observing the study cases shown in Figure 4A–E that ran at 300K, the first simulation shown allowed no gas molecules to pass using a nanoslit area estimated at ~144 Å$^2$. Moving on to a slightly higher nanoslit area (~171 Å$^2$,), in the simulation shown in Figure 4B, all $H_2$ molecules were able to exit the nanotube within the simulated 10 ns, most of them (95) having left within the first 3.0 ns. Thirteen $CH_4$ and one CO molecules were also able to exit the rotating nanotube. This case presented the highest number of $H_2$ molecules which exited the carbon nanotube out of all the investigated

situations. Although optimizing its selectivity is an obvious target for future studies building upon our novel design, captivating insights were observed given the behavior of the gases in this specific case.

As shown in Figure 7 and Supplementary Video S1, most gas molecules were placed in the central area of the rotating carbon nanotube, doubled by the second carbon nanotube wall for a length of 5 nm. Molecules with a smaller mass, mostly $H_2$ and $CH_4$, were able to leave for the two ends early on and easily pass into the filtrate area after a few collisions with the carbon nanocone at the end which allowed exiting. The bulk of the heavier molecules and the rest of the lighter molecules were found rotating slowly at the center of the nanotube (see Supplementary Video S1), slower than the imposed angular velocity. We think the observed phenomenon was due to the double-walled configuration, with some degree of adsorption to the inner wall taking place which could also be strengthened by the presence of the second wall. Thus, the slowing down of the rotational movement of the gas molecules could be observed while these remained at the center of the tube. This observation is valuable and should be investigated further as in this case all $H_2$ molecules were able to leave the tube by the end of the simulation time in spite of being caught in the bulk of molecules situated at the center of the nanotube. Interestingly, most $H_2$ molecules that exited the rotating carbon nanotube were found as if constantly being adsorbed and desorbed from the outer wall at the end of the simulation, as shown in Figure 4B, while also displaying rotational motion (see Supplementary Video S2). Again, this should be due to the combined effect of the rotating inner nanotube and the constant adsorption events on the outer nanotube. Thus, considering the length and placement of the double wall, it can act as a collector for gas molecules that have exited the rotating carbon nanotube. This observation holds especially for $H_2$ molecules as these were all found adsorbed on it at the end of the 10 ns, as opposed to the $CH_4$ molecules that exited, which were also found adsorbed on the graphene layers acting as walls for the setup.

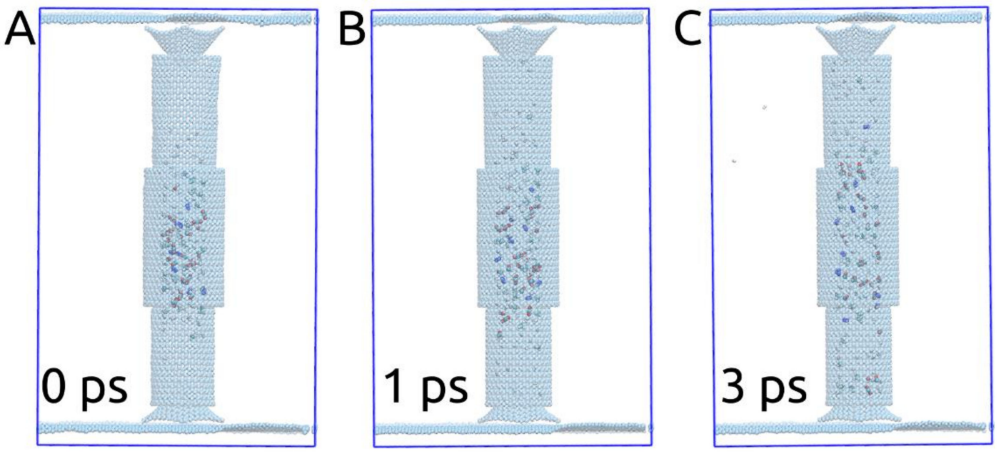


**Figure 7.** (**A**) Initial placement of the gas molecules inside the rotating carbon nanotube; (**B**) (1 ps) and (**C**) (3ps) The quick migration of the gas molecules towards the ends of the carbon nanotube.

Most exits through the free end of the rotating carbon nanotube relied on the gas molecules being "pushed out" by other nearby molecules. A change in the direction of movement was necessary due to the presence of the carbon nanocone (see Supplementary Video S3) and suggests that most molecules needed more energy to exit than they arrived with at the end of the nanotube. The change in the direction of movement followed due to collisions with the carbon nanocone and the rotating wall. In order to optimize selectivity and improve the overall performance of similar designs, future studies may use carbon nanocones of different disclinations.

Repositioning the cone by slightly moving it away from the nanotube and thus increasing the slit area, as in Figure 4C–E, leads to far less $H_2$ molecules being able to exit. In Figure 4C, only 11 $H_2$ molecules were able to exit the rotating nanotube, together with 2 $H_2O$ and 1 $CH_4$ molecules.

In contrast to the case discussed previously (Figure 4B), after 0.3 ns no more $H_2$ molecules exit or enter back into nanotube. Similarly, in Figure 4D, with the slight increase in the nanoslit area, 22 $H_2$ molecules were able to leave in the first 0.3 ns. In the simulation shown in Figure 4E, 24 $H_2$ molecules were able to exit. A peculiar event is observed in the 4D and 4E simulations: after some $H_2$ molecules exited early on, for the rest of the simulated time no more $H_2$ was able to exit, yet, surprisingly, most of the molecules that exited were able to come back into the nanotube from the filtrate area. This "come back" event is possible due to the disclination and orientation of the carbon nanocone to the nanotube: in these simulations it was positioned in such a way that when, eventually, a $H_2$ molecule that exited the rotating carbon nanotube collided with the cone it was deflected towards the nanotube (see Supplementary Video S3). In the simulation shown in Figure 4B, the positioning of the cone does not allow for the same phenomenon to happen.

### *3.5. 450K Study Cases*

Observing the cases shown in Figure 5A–E that ran at 450 K, no molecules were able to exit in the simulations shown in A and B with a nanoslit area of 144 Å$^2$ and 180 Å$^2$. Increasing the area slightly, to 218 Å$^2$, 10 $H_2$ molecules were able to exit within the simulated 5 ns. This case presented a very high selectivity, with $H_2$ molecules exiting constantly throughout the simulation. However, optimization to avoid $H_2$ getting stuck at the center of the rotating inner nanotube and an extension to the simulation are necessary to see whether the observations hold true for longer times and whether $H_2$ exit could be sped up. The current imposed angular velocity may play a role in preventing $H_2$ adsorption to the inner tube to some degree; however, experimentation with higher angular velocities would be beneficial.

Moving on to the final two cases, shown in Figure 5D,E, a similar phenomenon to that observed in Figure 4E was seen: initially, $H_2$ molecules exited the rotating nanotube, reaching a maximum number in the filtrate area within 0.1–0.2 ns; afterwards some of these are able to return into the rotating carbon nanocone. About 28 $H_2$ molecules leave in the simulation in Figure 5D and 50 leave in Figure 5E, with 20 and 48 returning by the end of the simulations. Most molecules that exited were able to find a way back. We think this phenomenon is dependent on the shape and disclination of the cone such that when a $H_2$ molecule in the filtrate area eventually collides with the carbon nanocone, it is deflected towards the interior of the rotating carbon nanotube (see Supplementary Video S3).

One important aspect to notice is that in most simulations presented, most gas molecules exit quickly, in the first 0.5 ns. The main outliers except those labeled "no filtrate" (Figures 4A and 5A,B) are presented in Figures 4B and 5C. The reason for the quick exit is, one may assume, the pressure build-up inside the tube; however, the observed phenomenon of gas molecules returning into the nanotube is somewhat interesting and may contradict this hypothesis.

Comparing the results obtained for similar areas at the two different temperatures by looking at Figure 4A–C and Figure 5A–C, a higher minimum nanoslit area was necessary to allow the passage of gas molecules. This aspect should be due to more vibration experienced by the carbon structure's atoms coming with the increased thermal energy of the system.

### *3.6. Total Flux*

To further characterize the gas separation performance of the investigated design, we estimated the flux of hydrogen molecules through the opening between the carbon nanocone and the end of the carbon nanotube allowing exiting. To calculate total flux, the number of $H_2$ crossings from both inside to outside and otherwise is taken into consideration. More precisely, the total flux can be calculated using the formula:

$$Flux = \frac{Crossings_{H_2}/N_A}{A_{opening} \times Time} \quad (1)$$

where the number of crossings of $H_2$ refers to the aforementioned number of crossings, $N_A$ is Avogadro's number and the area of the opening represents the area open for crossing at any one time. Although

we have calculated the available area for the molecules to escape the carbon nanotube through the Monte Carlo hit-and-miss procedures in Figures 4 and 5, this may not be the most representative model for this additional computation. The circular nanoslits formed in-between the carbon nanocones and the ends of the rotating carbon nanotube can be seen as two-segments nanochannels, shrinking in the first section and expanding afterwards. Essentially, once a gas molecule passes the height level of the carbon nanotube, the channel gets narrower as the carbon nanocone extends further upwards at an angle. Therefore, a molecule would have to traverse a slightly bent channel which it cannot do by solely maintaining its vertical direction. Considering the atom on the edge of the rotating carbon nanotube as a pivot point, the highest energy barrier for gas molecules is met when crossing the boundary line passing through the nanotube atom that is also perpendicular on the edge of the nanocone, be it directly on an atom or a bond. This is better displayed in Figure 8.

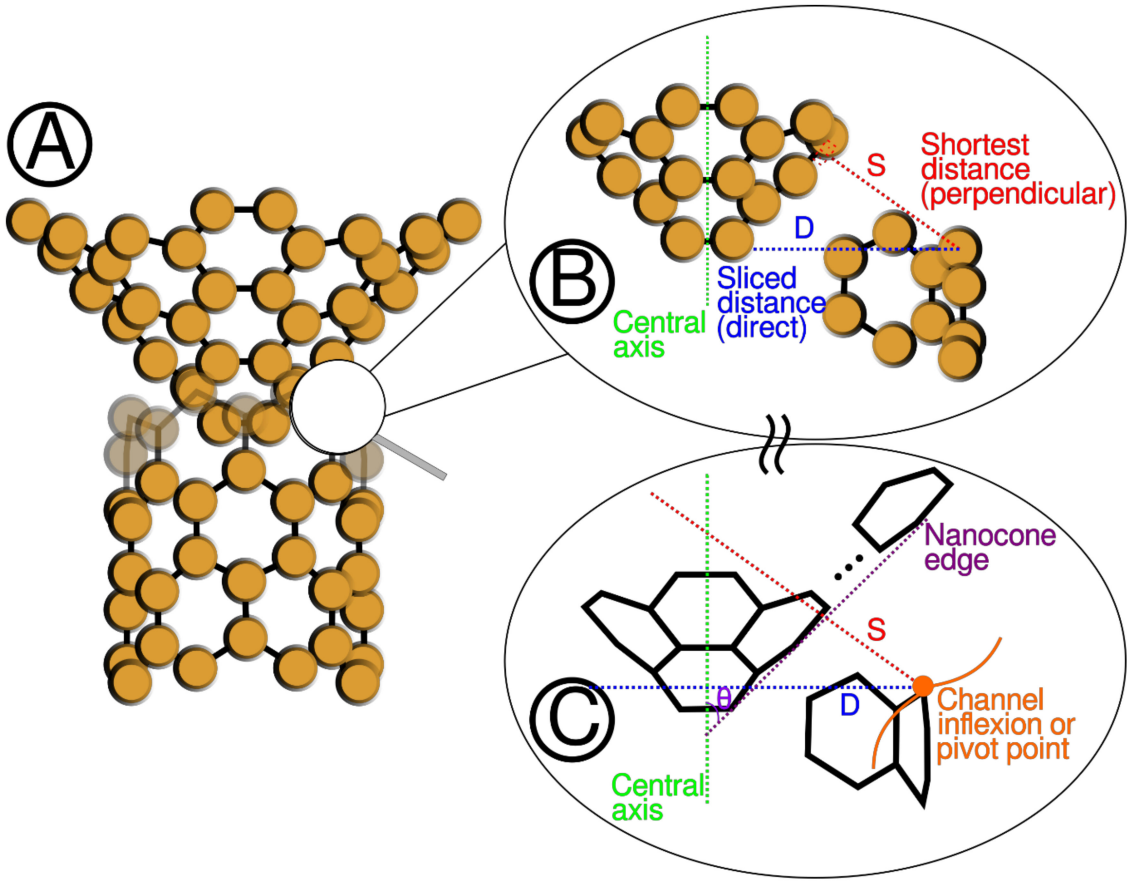


**Figure 8.** (**A**) Overview of the carbon nanocone and carbon nanotube edge assembly. (**B**) The characteristics and crossing points of the gap between carbon nanocone. (**C**) Schematic representation of the open nanochannel in between the two carbon allotropes and the mathematical approximation visually presented required to find the area for flux calculation.

In order to proceed towards total flux calculation, we approximated the carbon nanocone to have a circular base. Although the system has some slight variations among the structures' shapes due to the equilibration steps and imposed angular velocity, we assumed that both the carbon nanocone at any height level and the carbon nanotube are all circular.

Additionally, for mathematical simplicity, we considered both the rotating carbon nanotube and the carbon nanocone to be centered at the same point on the XY plane as shown in Figure 8. Consequently, the distance from the pivot point perpendicular to the carbon nanocone can be found through the following formula:

$$S = D \times sin(90 - \theta) \quad (2)$$

where $S$ represents the distance from the pivot point perpendicular to the carbon nanocone, $D$ represents the horizontal distance from the pivot point to the carbon nanocone and $\theta$ is half the apex angle of the carbon nanocone.

Given that all used carbon nanocones have a disclination angle of 120°, their apex angle at the tip is $2 \times sin^{-1}\left(1 - \frac{d_\theta}{360}\right)$ [37], where $_\theta$ is the disclination angle of the carbon nanocone and in this case the result of the formula is always 83.6°. The only remaining unknown is now distance $D$, which can be calculated from the areas found in Figures 4 and 5. Maintaining the consideration that both allotropes describe circular shapes, the determined area for each scenario can therefore be regarded as the difference between the area of a larger circle and a smaller one. Distance $D$ then corresponds to the difference between the radius of the carbon nanotube and the radius of the sliced carbon nanocone or the smaller circle, which can be easily found as:

$$D = \frac{\sqrt{A_{MC-CNT}}}{\pi} - \frac{\sqrt{A_{MC-CNT} - A_{nanoslit}}}{\pi} \tag{3}$$

where $A_{MC-CNT}$ represents the total area of the sectional carbon nanotube end and $A_{nanoslit}$ represents the area of the nanoslit found through the Monte Carlo hit-and-miss procedure. This result can now be introduced into the equation to find distance $S$. However, in order to find the area that can correctly be used to determine the flux, it is necessary to pretend to have an imaginary open nanocone made up of all the perpendicular lines starting from any point on the edge of the carbon nanotube and ending on the carbon nanocone. Therefore, this area can now be calculated as the surface area of an open cone, which is the formula of the difference between the surface areas of two closed cones. More exactly, this is:

$$\begin{aligned} A_{opening} = \pi \times & \left(\sqrt{\frac{A_{MC-CNT}}{\pi}} \times \frac{1}{cos\theta} \times \sqrt{\frac{A_{MC-CNT}}{\pi}}\right) \\ -\pi \times & \left(\sqrt{\frac{A_{MC-CNT}}{\pi}} \times \frac{1}{cos\theta} - S\right) \times \left(\sqrt{\frac{A_{MC-CNT}}{\pi}} - Scos\theta\right) \end{aligned} \tag{4}$$

where $A_{opening}$ is the required area of the opening from the flux formula, $A_{MC\text{-}CNT}$ represents the total area of the section carbon nanotube end and $\theta$ is half the apex angle of the carbon nanocone and $S$ is the distance from a pivot point on the edge of the carbon nanotube perpendicular to the carbon nanocone. Alternatively, we have determined an alternative flux which uses the entire area of the carbon nanotube's open end in its computation. In addition, because much of the flow to the outside of the prototype takes place before reaching 3 ns in many simulations, we have also worked out the flux up until that point in time. Therefore, the final calculations for flux lead to the results displayed in Figure 9.

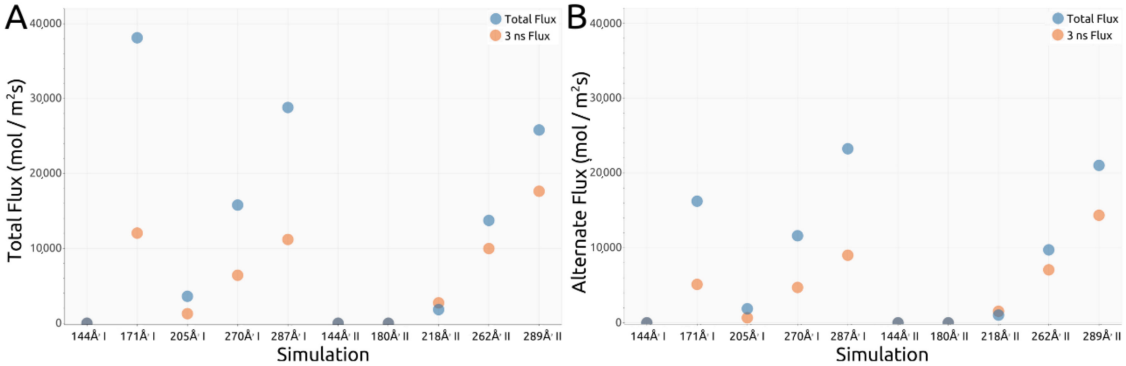


**Figure 9.** (**A**) Total flux of each simulation, together with a 3-ns flux calculation; (**B**) alternate flux of each simulation, together with a 3-ns alternate flux calculation.

Looking at Figure 9A, regarding the total flux values, at 300 K the special case, shown in Figure 4B, in which all $H_2$ molecules were able to exit through the nanoslit stands as an outlier, having the highest

flux value out of the 300 K simulations. Curiously, for the next three simulations, each with a slightly increased nanoslit area, a trend can be seen as flux increases with the increased area. For the 450 K simulations, the first two areas (144 Å$^2$ and 180 Å$^2$) have a flux of 0 mol/m$^2$s as no molecules were able to pass into the filtrate area, while the following three show the same trend of flux increasing with increased area. These observations pin-point the simulation presented in Figure 4B as a special case and show that obtaining desirable outcomes with this setup is a complex endeavor dependent on a multitude of factors such as the disclination of the carbon nanocone, its orientation and the created nanoslit area. Similar aspects can be observed in the 3 ns-flux calculations. The slope of the trend of increasing flux is higher than in the case of total flux, which is expected given that most of the crossings take place early on. An important aspect to notice however, is that in the last three cases shown for 300 K and last three cases shown for 450 K, some of the flux is generated by the gas molecules that cross back into the tube, which is an interesting, yet detrimental effect to be investigated in future studies. The alternate flux values, presented in Figure 9B, display similar trends to those shown in Figure 9A, yet due to the increased area value in the calculation the values are significantly smaller.

The calculated fluxes compare with predicted values from other computational studies investigating carbon-based membranes. For example, in the best performing simulation, the total flux is equivalent to the one observed for a pore created on a 3 nm × 3 nm graphene sheet with the size of 16 removed carbon atoms [20]. When considering the same scenario's flux in the first 3 ns, the value goes much higher as most of the hydrogen molecules already exited through the end of the carbon nanotube. This flux exceeds that of a graphene nanopore equivalent to the size of 28 removed carbon atoms. Alternatively, if we are to consider the alternate versions of total and 3 ns $H_2$ flux, the values diminish by a factor of about 2.35 and reach equivalence with a pore of 12- and respectively, 20-removed carbon atoms on the aforementioned graphene sheet. Optimizing $D$ and $S$ values is a target for future investigations, both with regards to flux and selectivity, for achieving an enhanced gas separation performance. We have obtained favorable results indicating high hydrogen selectivity in the case presented in Figure 5C at 450 K, with $D$ = 4.35 Å and $S$ = 3.25 Å. Table 1 displays the calculated variables for the flux computations, including all the aforementioned flux versions.

**Table 1.** Variables for flux computations.

| Simulation | $H_2$ Crossings | $D$ (Å) | $S$ (Å) | $A_{nanoslit}$ (Å$^2$) | $A_{opening}$ (Å$^2$) | Total $H_2$ Flux (mol/m$^2$s) | 3 ns $H_2$ Flux (mol/m$^2$s) | Alternate $H_2$ Flux (mol/m$^2$s) | Alternate 3 ns $H_2$ Flux (mol/m$^2$s) |
|---|---|---|---|---|---|---|---|---|---|
| 144 Å$^2$ I | 0 | 2.59 | 1.93 | 144 | 114 | 0 | 0 | 0 | 0 |
| 171 Å$^2$ I | 100 | 3.18 | 2.37 | 171 | 138 | 12,035 | 38,112 | 5125 | 16,230 |
| 205 Å$^2$ I | 13 | 3.99 | 2.98 | 205 | 169 | 1276 | 3598 | 666 | 1879 |
| 270 Å$^2$ I | 92 | 6.00 | 4.47 | 270 | 239 | 6404 | 15,779 | 4715 | 11,617 |
| 287 Å$^2$ I | 176 | 6.74 | 5.02 | 287 | 261 | 11,183 | 28,806 | 9020 | 23,234 |
| 144 Å$^2$ II | 0 | 2.59 | 1.93 | 144 | 114 | 0 | 0 | 0 | 0 |
| 180 Å$^2$ II | 0 | 3.39 | 2.52 | 180 | 146 | 0 | 0 | 0 | 0 |
| 218 Å$^2$ II | 15 | 4.35 | 3.25 | 218 | 182 | 2731 | 1821 | 1538 | 1025 |
| 262 Å$^2$ II | 69 | 5.73 | 4.27 | 262 | 230 | 9972 | 13,729 | 7073 | 9738 |
| 289 Å$^2$ II | 140 | 6.82 | 5.08 | 289 | 264 | 17,622 | 25,803 | 14,351 | 21,013 |

## 4. Conclusions

We presented a novel design based on a partial double-walled rotating carbon nanotube–carbon nanocone complex and investigated its performance in terms of hydrogen gas separation from a gas mixture containing $H_2$, $CH_4$, CO, $CO_2$, $N_2$ and $H_2O$ molecules. The rotational motion generated using an imposed angular velocity was meant to resemble the recently observed motion of double walled carbon nanotubes exposed to electric fields [3]. Although needing improvements, the new design was found capable of high selectivity for $H_2$ and novel insights were observed to help improve future membrane or nanomotor designs for gas separation. Due to its uniqueness, we consider it will open up the interest of many researchers looking to experiment with Molecular Dynamics simulations for

filtration applications and provide a starting point for new daring designs. We have highlighted the importance of the carbon nanocone's disclination and positioning relative to the carbon nanotube and shown it can greatly impact the outcome of the filtration process, especially since in some interesting cases gas molecules were found capable to return into the nanotube. Although not yet developed experimentally, we deem this kind of setup and in silico investigation aids towards such goals by highlighting both the advantages such as the simplicity of the design and disadvantages such as the tight control one would need over the positioning of the carbon nanocones relative to the carbon nanotube. In future studies we aim to experiment with different cone disclinations to further optimize our findings and improve on our presented setup.

**Supplementary Materials:** The following are available online at http://www.mdpi.com/2079-6412/10/12/1207/s1, Video S1. SV showing the initial placement of the gas molecules in the central double-walled carbon nanotube area, the early departure of the lighter gas molecules towards the two ends of the nanotube and the bulk of gas molecules found to rotate slowly with the inner tube. Taken from a simulation at 300K; Video S2. SV showing the most of the H2 molecules that exited the rotating carbon nanotube to be in the vicinity of the outer wall of the double-walled section of the nanotube, as if constantly adsorbed and desorbed, while still displaying some rotational motion. Taken from a simulation at 300 K; Video S3. SV showing the re-entering of one $H_2$ molecule into the rotating carbon nanotube. Taken from a simulation at 300 K.

**Author Contributions:** Conceptualization, S.M. (Sorin Muraru), S.M. (Sebastian Muraru) and M.I.; methodology, S.M. (Sorin Muraru) and S.M. (Sebastian Muraru).; software, S.M. (Sorin Muraru) and S.M. (Sebastian Muraru); validation, S.M. (Sorin Muraru) and S.M. (Sebastian Muraru); formal analysis, S.M. (Sorin Muraru) and S.M. (Sebastian Muraru); investigation, S.M. (Sorin Muraru), S.M. (Sebastian Muraru) and M.I.; resources, M.I.; data curation, S.M. (Sorin Muraru) and S.M. (Sebastian Muraru); writing—original draft preparation, S.M. (Sorin Muraru) and S.M. (Sebastian Muraru); writing—review and editing, S.M. (Sorin Muraru), S.M. (Sebastian Muraru) and M.I.; visualization, S.M. (Sorin Muraru) and S.M. (Sebastian Muraru); supervision, M.I.; project administration, M.I.; funding acquisition, M.I. All authors have read and agreed to the published version of the manuscript.

**Funding:** This work was supported by a grant of the Executive Agency for Higher Education, Research, Development and innovation funding (UEFISCDI), project number PN-III-P1-1.1-TE-2016-24-2, contract TE 122/2018.

**Conflicts of Interest:** The authors declare no conflict of interest.

## References

1. Winter, M.; Brodd, J.R. What Are Batteries, Fuel Cells, and Supercapacitors? *Chem. Rev.* **2004**, *104*, 4245–4270. [CrossRef] [PubMed]
2. Bernardo, G.; Araújo, T.; da Silva Lopes, T.; Sousa, J.; Mendes, A. Recent advances in membrane technologies for hydrogen purification. *Int. J. Hydrogen Energy* **2020**, *45*, 7313–7338. [CrossRef]
3. Bailey, S.W.D.; Amanatidis, I.; Lambert, C.J. Carbon Nanotube Electron Windmills: A Novel Design for Nanomotors. *Phys. Rev. Lett.* **2008**, *100*, 256802. [CrossRef] [PubMed]
4. Wang, Y.; Wang, W.; Zhu, S.; Guo, L.; Zhang, Z.; Li, P. The mechanisms study of the porous graphene for the purification of the mixed gases: A multi-scale computational method. *Comput. Mater. Sci.* **2018**, *143*, 277–285. [CrossRef]
5. Esfandiarpoor, S.; Fazli, M.; Ganji, M.D. Reactive molecular dynamic simulations on the gas separation performance of porous graphene membrane. *Sci. Rep.* **2017**, *7*, 16561. [CrossRef]
6. Yuan, Z.; Rajan, A.G.; Misra, R.P.; Drahushuk, L.W.; Agrawal, K.V.; Strano, M.S.; Blankschtein, D. Mechanism and Prediction of Gas Permeation through Sub-Nanometer Graphene Pores: Comparison of Theory and Simulation. *ACS Nano* **2017**, *11*, 7974–7987. [CrossRef]
7. Zheng, H.; Zhu, L.; He, D.; Guo, T.; Li, X.; Chang, X.; Xue, Q. Two-dimensional graphene oxide membrane for $H_2/CH_4$ separation: Insights from molecular dynamics simulations. *Int. J. Hydrogen Energy* **2017**, *42*, 30653–30660. [CrossRef]
8. Liu, Q.; Gupta, K.M.; Xu, Q.; Liu, G.; Jin, W. Gas permeation through double-layer graphene oxide membranes: The role of interlayer distance and pore offset. *Sep. Purif. Technol.* **2019**, *209*, 419–425. [CrossRef]
9. Wang, P.; Li, W.; Du, C.; Zheng, X.; Sun, X.; Yan, Y.; Zhang, J. $CO_2/N_2$ separation via multilayer nanoslit graphene oxide membranes: Molecular dynamics simulation study. *Comput. Mater. Sci.* **2017**, *140*, 284–289. [CrossRef]

10. Wang, S.; Dai, S.; Jiang, D. Continuously Tunable Pore Size for Gas Separation via a Bilayer Nanoporous Graphene Membrane. *Appl. Nano Mater.* **2019**, *2*, 379–384. [CrossRef]
11. Raghavan, B.; Gupta, T. $H_2/CH_4$ Gas Separation by Variation in Pore Geometry of Nanoporous Graphene. *J. Phys. Chem. C* **2017**, *121*, 1904–1909. [CrossRef]
12. Sun, C.; Wen, B.; Bai, B. Application of nanoporous graphene membranes in natural gas processing: Molecular simulations of $CH_4/CO_2$, $CH_4/H_2S$ and $CH_4/N_2$ separation. *Chem. Eng. Sci.* **2015**, *138*, 616–621. [CrossRef]
13. Wang, S.; Tian, Z.; Dai, S.; Jiang, D. Effect of pore density on gas permeation through nanoporous graphene membranes. *Nanoscale* **2018**, *10*, 14660–14666. [CrossRef] [PubMed]
14. Wang, Y.; Yang, Q.; Zhong, C.; Li, J. Theoretical investigation of gas separation in functionalized nanoporous graphene membranes. *Appl. Surf. Sci.* **2017**, *407*, 532–539. [CrossRef]
15. Jiang, D.; Cooper, V.R.; Dai, S. Porous Graphene as the Ultimate Membrane for Gas Separation. *Nano Lett.* **2009**, *9*, 4019–4024. [CrossRef] [PubMed]
16. Hughes, Z.E.; Walsh, T.R. Computational Chemistry for Graphene-based Energy Applications: Progress and Challenges. *Nanoscale* **2015**, *7*, 6883–6908. [CrossRef]
17. Ye, H.; Li, D.; Ye, X.; Zheng, Y.; Zhang, Z.; Zhang, H.; Chen, Z. An adjustable permeation membrane up to the separation for multicomponent gas mixture. *Sci. Rep.* **2019**, *9*, 7380. [CrossRef]
18. Sun, C.; Bai, B. Fast mass transport across two-dimensional graphene nanopores: Nonlinear pressure-dependent gas permeation flux. *Chem. Eng. Sci.* **2017**, *165*, 186–191. [CrossRef]
19. Shan, M.; Xue, Q.; Jing, N.; Ling, C.; Zhang, T.; Yan, Z.; Zheng, J. Influence of chemical functionalization on the $CO_2/N_2$ separation performance of porous graphene membranes. *Nanoscale* **2012**, *4*, 5477. [CrossRef]
20. Sun, C.; Boutilier, M.S.H.; Au, H.; Poesio, P.; Bai, B.; Karnik, R.; Hadjiconstantinou, N.G. Mechanisms of Molecular Permeation through Nanoporous Graphene Membranes. *Langmuir* **2014**, *30*, 675–682. [CrossRef]
21. Wesołowski, R.P.; Terzyk, A.P. Pillared graphene as a gas separation membrane. *Phys. Chem. Chem. Phys.* **2011**, *13*, 17027. [CrossRef] [PubMed]
22. Jiao, S.; Xu, Z. Selective Gas Diffusion in Graphene Oxides Membranes: A Molecular Dynamics Simulations Study. *ACS Appl. Mater. Interfaces* **2015**, *7*, 9052–9059. [CrossRef] [PubMed]
23. Zhu, L.; Xue, Q.; Li, X.; Jin, Y.; Zheng, H.; Wu, T.; Guo, Q. Theoretical Prediction of Hydrogen Separation Performance of Two-Dimensional Carbon Network of Fused Pentagon. *ACS Appl. Mater. Interfaces* **2015**, *7*, 28502–28507. [CrossRef] [PubMed]
24. Muraru, S.; Ionita, M. Super Carbonaceous Graphene-based structure as a gas separation membrane: A Non-Equilibrium Molecular Dynamics Investigation. *Compos. B Eng.* **2020**, *196*, 108140. [CrossRef]
25. Boretti, A.; Al-Zubaidy, S.; Vaclavikova, M.; Al-Abri, M.; Castelletto, S.; Mikhalovsky, S. Outlook for graphene-based desalination membranes. *NPJ Clean Water* **2018**, *1*, 5. [CrossRef]
26. Roy, K.; Mukherjee, A.; Maddela, N.R.; Chakraborty, S.; Shen, B.; Li, M.; Du, D.; Peng, Y.; Lu, F.; Garcia Cruzatty, L.C. Outlook on the bottlenecks of carbon nanotube in desalination and membrane-based water treatment—A review. *J. Environ. Chem. Eng.* **2020**, *8*, 103572. [CrossRef]
27. JCrystalSoft. Nanotube Modeler: Generation of Nano-Geometries. Available online: https://www.jcrystal.com (accessed on 10 August 2020).
28. Abraham, M.J.; Murtola, T.; Schulz, R.; Páll, S.; Smith, J.C.; Hess, B.; Lindahl, E. GROMACS: High performance molecular simulations through multi-level parallelism from laptops to supercomputers. *SoftwareX* **2015**, *1–2*, 19–25. [CrossRef]
29. Jorgensen, W.L.; Maxwell, D.S.; Tirado-Rives, J. Development and Testing of the OPLS All-Atom Force Field on Conformational Energetics and Properties of Organic Liquids. *J. Am. Chem. Soc.* **1996**, *118*, 11225–11236. [CrossRef]
30. Mark, P.; Nilsson, L. Structure and Dynamics of the TIP3P, SPC, and SPC/E Water Models at 298K. *J. Phys. Chem. A* **2001**, *105*, 9954–9960. [CrossRef]
31. Bussi, G.; Donadio, D.; Parrinello, M. Canonical sampling through velocity-rescaling. *J. Chem. Phys.* **2007**, *126*, 014101. [CrossRef]
32. Lemkul, J. From Proteins to Perturbed Hamiltonians: A Suite of Tutorials for the GROMACS-2018 Molecular Simulation Package. *LiveCoMS* **2019**, *1*, 5068. [CrossRef]
33. Chen, J.; Wang, X.; Dai, C.; Chen, S.; Tu, Y. Adsorption of GA module onto graphene and graphene oxide: A molecular dynamics simulation study. *Physica E Low Dimens. Syst. Nanostruct.* **2014**, *62*, 59–63. [CrossRef]

34. Bokeh Development Team. Bokeh: Python Library for Interactive Visualization. Available online: https://bokeh.org (accessed on 21 September 2020).
35. Gowers, R.J.; Linke, M.; Barnoud, J.; Reddy, T.J.E.; Melo, M.N.; Seyler, S.L.; Domanski, J.; Dotson, D.L.; Buchoux, S.; Kenney, I.M.; et al. MDAnalysis: A Python Package for the Rapid Analysis of Molecular Dynamics Simulations. In Proceedings of the 15th Python in Science Conference (SciPy), Austin, TX, USA, 11–17 July 2016; pp. 98–105. [CrossRef]
36. Tu, Q.; Yang, Q.; Wang, H.; Li, S. Rotating carbon nanotube membrane filter for water desalination. *Sci. Rep.* **2016**, *6*, 26183. [CrossRef] [PubMed]
37. Ansari, R.; Momen, A.; Rouhi, S.; Ajori, S. On the Vibration of Single-Walled Carbon Nanocones: Molecular Mechanics Approach versus Molecular Dynamics Simulations. *Shock Vib.* **2014**, *2014*. [CrossRef]